

Periodic Variability in Space Photometry of 181 New Supermassive Black Hole Binary Candidates

P. Huijse^{1,2*}, J. Davelaar^{3,4}, J. De Ridder¹, N. Jannsen¹, C. Aerts^{1,5,6}

¹Institute of Astronomy, KU Leuven, Celestijnenlaan 200D, B-3001 Leuven, Belgium.

²Millennium Institute of Astrophysics Nuncio Monseñor Sotero Sanz 100, Of. 104, Providencia, Santiago, Chile.

³Department of Astrophysical Sciences, Princeton University, Peyton Hall, Princeton, 08544, New Jersey, USA.

⁴NASA Einstein Fellow.

⁵ Department of Astrophysics, IMAPP, Radboud University Nijmegen, PO Box 9010, 6500 GL, Nijmegen, The Netherlands.

⁶Max Planck Institute for Astronomy, MPIA, Koenigstuhl 17, 69117, Heidelberg, Germany.

Contributing authors: pablo.huijse@kuleuven.be; jdavelaar@princeton.edu; joris.deridder@kuleuven.be; nicholas.jannsen@kuleuven.be; conny.aerts@kuleuven.be;

Abstract

Robust detections of supermassive black hole binaries (SMBHBs) are essential to unravel the role of galaxy mergers in galaxy evolution and for identifying potential sources of low-frequency gravitational waves. One of the most commonly used observational signatures of SMBHBs is periodic variability in the light curves of active galactic nuclei (AGN), which may arise from accretion rate modulation or relativistic Doppler boosting due to binary orbital motion. However, intrinsic stochastic AGN variability can mimic such periodic signals, complicating robust identification. We report the discovery of 181 new SMBHB candidates from a sample of approximately 770,000 AGN observed by the *Gaia* space observatory. Periodic signals were identified using a novel and computationally efficient Bayesian model selection framework, enabling unbiased source selection and quantifying the likelihood of periodicity over stochastic variability. These candidates nearly double the known SMBHB population and provide a prioritized target list for next-generation time-domain surveys.

Supermassive black hole binaries (SMBHBs) form through galactic mergers and play a crucial role in the evolution of their host galaxies [1]. As their orbital separation decreases due to dynamical friction with surrounding stars and gas, the binary eventually begins emitting gravitational waves, leading to an inevitable merger. The low-frequency gravitational waves from these systems are expected to be detected by the future space mission LISA [2, 3] and by pulsar timing arrays [4–7]. However, these facilities provide poor sky localization, making it challenging to pinpoint the host galaxies. Distinctive electromagnetic signatures are therefore used to identify SMBHB candidates. A promising approach is detecting periodic variability in the light curves of active galactic nuclei (AGN), driven either by accretion rate modulation due to binary orbital motion [8–10] or by relativistic Doppler boosting or self-lensing [11–13].

In the past decade, large-scale time-domain surveys have facilitated systematic searches for SMBHBs by identifying periodic signatures in AGN light curves. In the optical, the Catalina Real-time Transient Survey (CRTS) identified 111 candidates [14], while the Palomar Transient Factory (PTF)

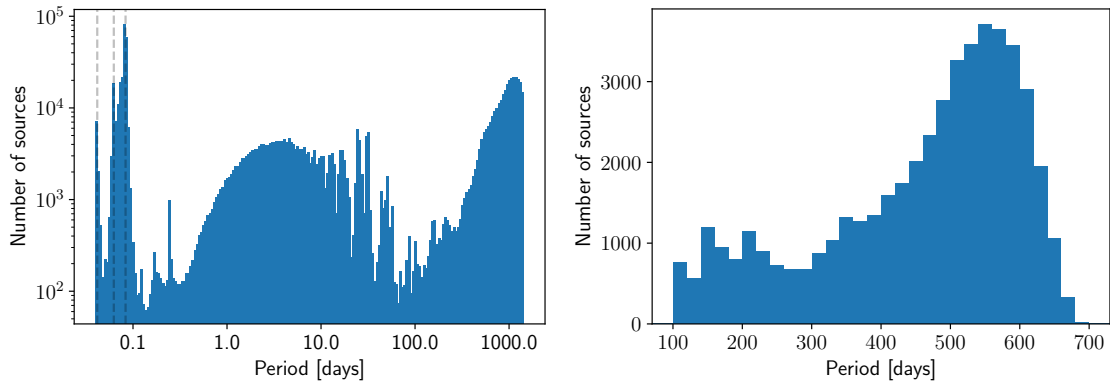


Fig. 1 Left panel: Histogram of the dominant periods from a Lomb-Scargle periodogram for 770,110 selected *Gaia* AGN sources (logarithmic bins). The dashed lines are periodicities associated with *Gaia*'s scanning law. Right panel: Histogram for the subset of 48,472 sources after removing periods below 100 days and longer than 150% of the light curve duration.

found 50 candidates, later decreased to 33 when incorporating CRTS data [15]. A study of Pan-STARRS1 sources identified one significant candidate [16, 17], and an additional three sources by ZTF [18]. In the case of OJ287, a large non-thermal flare is observed every 16 years, which is attributed to a secondary black hole colliding with the primary accretion flow [19]. Similar periodicities have also been discovered in the ultraviolet (UV) light curves of e.g. PG1302 [20], and in the jet orientation of M81 [21, 22]. The total set of potential SMBHB candidates currently stands at approximately 200 sources. Upcoming large time-domain surveys such as LSST [23] and Roman [24] are expected to uncover many more in the coming years. Here we explore the vast archival dataset offered by the *Gaia* space mission [25] that remains largely unexplored so far in terms of SMBHB. Given that *Gaia* photometry turned out to be powerful to uncover periodic phenomena far beyond its original goals [26], it offers a timely opportunity to expand the known population of SMBHB candidates.

The *Gaia* space telescope has surveyed the full sky since 2013, providing astrometric, photometric, and spectroscopic data. While the main focus of *Gaia* is to survey objects in our own galaxy, background AGN are repeatedly observed as a byproduct. *Gaia* Data Release 3 (DR3) [27] includes 6.6 million quasar (QSO) candidates [28], with one million of them featuring epoch photometry covering 34 months of data. The upcoming *Gaia* DR4 (expected in 2026) will extend the observational baseline to 66 months. A subset, *Gaia*-CRF3, has been cross-matched with other known AGN/QSO catalogues [29].

Although apparent periodicity in AGN light curves is a promising indicator of SMBHBs, AGN without a binary component also exhibit stochastic variability across a broad range of timescales [30]. This variability arises from turbulent fluctuations in the accretion flow and is well characterised by a red noise power spectrum, where power decreases as a function of frequencies, making long-period variations prominent. As a result, apparent periodicity can often be misinterpreted and render conventional False Alarm Probabilities (FAPs) insufficient for SMBHB identification [31, 32]. To model the stochastic behaviour of AGN light curves, several studies have found that the Damped Random Walk (DRW) model¹ provides a reasonable statistical description of the observed variability [30, 33–35], although modelling limitations have been noted at time-scales of three months and less [36, 37]. Here, we apply both FAP and DRW to *Gaia* AGN light curves, and we limit the search to time-scales for which the DRW model is valid.

The first step of our analysis is to refine the *Gaia* AGN sample. We apply initial cuts based on photometric completeness, cross-matching with *Gaia*-CRF3, and removing sources with unreliable or local red-shifts, spurious variability due to *Gaia*'s scanning law, or classification as periodic variable stars [29, 38, 39] (see Methods for details). This filtering reduces the sample to 770,110 candidates, considering only *G* band photometry. We then compute Lomb-Scargle (LS) periodograms for each source (see Methods). The distribution of peak LS periods for the 770,110 selected sources is shown in Figure 1 left panel, with dashed lines indicating 12, 16, and 24 cycles per day, corresponding to frequencies linked to *Gaia*'s scanning law [38].

Following [40], we limit our SMBHB candidate search to periods longer than 100 days. Shorter periods are unlikely to represent genuine detections, as the odds of observing the binary in late

¹Also known as the Ornstein–Uhlenbeck process.

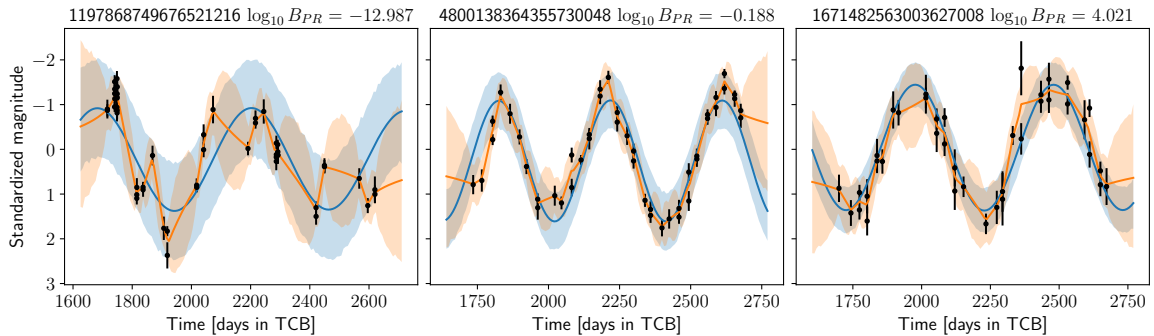


Fig. 2 Examples of *Gaia* DR3 light curves of AGN fitted with periodic (blue) and stochastic (orange) models. Measurements and their errors are shown in black. The *Gaia* source identifier and the Bayes factor $\log_{10} B_{PR}$ are displayed in the title, where lower values of the latter stand for weaker evidence of periodic variability.

evolutionary stages close to a merger drop with decreasing period due to the rapid in-spiral timescales driven by gravitational waves. Additionally, we require at least 1.5 cycles to be observed within the duration of the light curve, setting a maximum period of $P_{\max} = T/1.5$, where T is the observation span (941 days on average). These stringent constraints reduce the sample to 48,472 sources.

As a first step in hunting for periodic variability of our potential SMBHB candidates, we compute the FAP as defined by [41]. We find that 92.1% and 82.5% of sources exhibit significant periodic variability at $\text{FAP} < 0.01$ and < 0.001 , respectively. As shown in Figure 1 right panel, the estimated period distribution is skewed towards long timescales, which is consistent with red-noise-dominated variability as pointed out by [31]. Periodogram FAPs are designed to distinguish sinusoidal variations from Gaussian white noise, not accounting for non-Gaussian errors or stochastic variability, the latter being expected for AGN. Therefore, a more robust approach is necessary to distinguish genuine periodic variability from stochastic signals. Following [31], [42] and [32] we apply a Bayesian model selection approach to compare two competing hypotheses as best model for the observed variability:

- \mathcal{H}_P (Periodic): a sinusoidal model;
- \mathcal{H}_R (Red noise): a Damped Random Walk (DRW) model.

Both hypotheses are tested using Gaussian Processes (GPs), where the parameters for the 48,472 selected sources are inferred using a Markov Chain Monte Carlo (MCMC) approach (see Methods). A total of 66 sources were removed due to inadequate MCMC convergence, yielding 48,406 properly modelled sources. The inferred posteriors are used to estimate the Bayes factor B_{PR} , which stands for the ratio between the Bayesian evidence of \mathcal{H}_P versus \mathcal{H}_R (see Methods). Figure 2 shows three example *Gaia* AGN light curves with the median of the predictive GP posterior (solid line) for the periodic (blue) and DRW (orange) models. The shaded area covers 90% of the predictive posterior.

Figure 3 presents the distribution of $\log_{10} B_{PR}$ (in blue) for the 48,406 sources. We find that the periodic model is favoured over the stochastic variability model for 10.86% of the sources, at a level of $\log_{10} B_{PR} > 0$. To establish a robust threshold for the Bayes factor, we adopt a simulation-based approach (see Methods). The (null) distribution of the Bayes factor for a set of 89,248 simulated light curves based on the DRW model with LS periods within the range 100 - $T/1.5$ days is shown in orange in Figure 3. The 99.9th percentile of the null distribution is shown with a dashed line and occurs at $\log_{10} B_{PR} = 3.0423$. We use this value as a conservative threshold to select those sources among the 48,406 which are dominated by periodic variability. This leads to a final selection of 181 SMBHB candidates. Figure 4 presents the *Gaia* light curves for three of them. Additional examples are presented in Figure A1. A total of 148 (81.8%) of the candidates have a period in $[T/2.5, T/1.5]$ days. Examples from the 33 SMBHB candidates with periods $< T/2.5$ (~ 370 days) are shown in Figure A2. The full list of sources and their Bayes factors is published in the accompanying GASP (*Gaia* AGN Survey of Periodic variability) catalogue. GASP provides the largest sample of SMBHB candidates to date and will be the primary reference target list for upcoming time-domain surveys and multi-messenger astrophysics. As an additional verification, we reevaluate the 181 candidates using a red noise model with a steeper high-frequency slope as null hypothesis. Appendix B demonstrates that the periodic model remains as the most strongly supported in this scenario. Cross-checking with previous studies reveals that there is no overlap between our 181 candidates and those identified by [14, 15, 18, 43]. Of the 99 candidates in the literature present in our initial *Gaia* selection, only 9 have

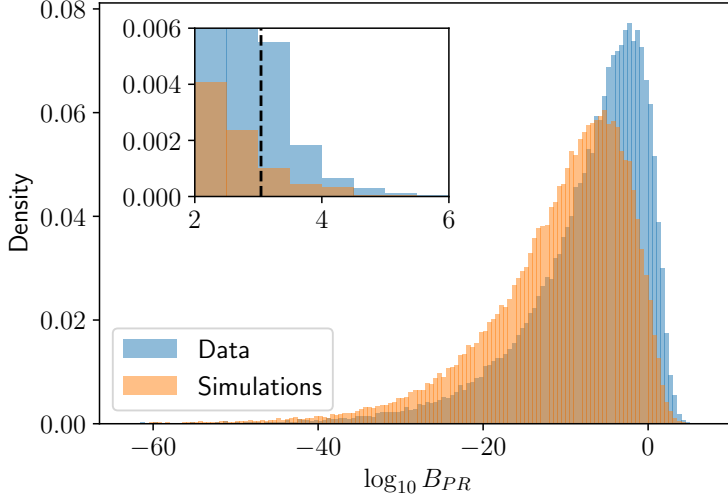


Fig. 3 Distribution of the logarithmic Bayes factor for the *Gaia* sample and for simulations. The blue histogram represents the 48,406 observed *Gaia* AGN time series. The orange distribution corresponds to 89,248 simulated light curves relying on a DRW model representing stochastic variability. The embedded sub-figure details the right tail of the distributions, where the dashed line indicates 99.9% of the simulated data distribution.

estimated periods between 100 and P_{\max} days. In these 9 cases, DRW is favoured over periodicity, however, DR4 and DR5 will be needed to fully rule out or confirm this, as in most cases the literature period exceeds the span of DR3.

Previous works have modelled SMBHBs as a periodic signal superimposed on DRW noise [17, 32, 42]. However, simulation tests applying this model on *Gaia* DR3 sampling and 34-month baseline reveal that it is not possible to find a threshold to discern candidates. A similar result was obtained by [32] using LSST simulations, where they demonstrate that, unless the red-noise-driven variability contributes minimally to the light curve, candidates with short periods relative to the survey baseline cannot be reliably recovered. By instead using a less flexible periodic model that does not include red noise, we are imposing a purity-driven criterion to reduce false detections maximally, acknowledging the potential under-selection of true candidates where red noise and periodic variability are comparable. This decision should be revisited once extended data from future data releases are available.

Given the limitations of DR3 and following [31], reassessment of these results with data from LSST, Roman, and upcoming data releases 4 and 5 of *Gaia* will be done in the future. We simulated 40,000 DRW time series with the DR4 time span of 5.5 years for a pure DRW model to illustrate the impact of extended *Gaia* data on binarity detection. The results reveal a significant improvement on the ability to distinguish SMBHBs with dominant periodic over stochastic variability (see Methods). As the next generation of large time-domain surveys will provide long-term monitoring of up to 100 million AGN, our GASP sources could serve as prime targets for early follow-up. The identification of SMBHBs will bring us closer to detecting supermassive black hole mergers, and help unveil the role of SMBHBs in galaxy evolution over cosmological timescales.

Methods

Initial AGN sample

Our initial sample is composed of the 6,649,162 sources from the DR3 `qso_candidates` table [28]. We limit this sample to sources with published photometric time series having at least 20 observations in the *Gaia* *G* band. This initial filtering reduces the dataset to 1,048,769 sources. We further constrain the sample by requiring the sources to be in the *Gaia*-CRF3, ensuring that they appear in at least one of 17 quasars and AGN catalogues cross-matched to construct the CRF3 table [29]. This criterion narrowed the candidate list to 787,197 sources.

Subsequently, we apply a conservative filter based on the redshifts estimated by the *Gaia* Quasar Classifier (QSOC) module, excluding 5,283 sources with $z < 0.1$ and 11,302 sources that lack redshift information. We also use two statistics from [38], namely the Spearman correlation and the significance of the scan angle signal, to remove 163 sources whose variability is affected by *Gaia*'s

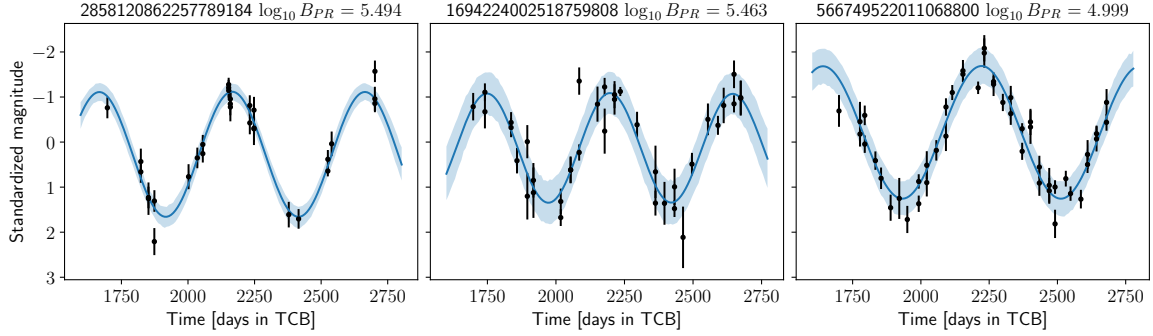


Fig. 4 Three *Gaia* sources with Bayes factors above the simulation-based threshold. The GP posterior with a periodic covariance is shown in blue, where the solid line represents the median prediction and the shaded region denotes the 90% credible interval. Data is shown in black. Illustration of additional candidates can be found in Appendix A.

scanning law. Additionally, we exclude 339 sources classified as periodic variable stars by [39]. These filtering steps result in a final sample of 770,110 sources. The source identifiers of this sample can be retrieved with the following ADQL query:

```
SELECT qso.source_id
FROM gaiadr3.qso_candidates
AS qso
JOIN gaiadr3.vari_spurious_signals
AS spurious USING (source_id)
WHERE spurious.num_obs_g_fov >= 20
AND qso.gaia_crf_source='t'
AND qso.redshift_qsoc>0.1
AND (spurious.spearman_corr_ipd_g_fov<0.8
OR spurious.scan_angle_model_ampl_sig_g_fov<6)
AND (qso.vari_best_class_name = 'AGN'
OR qso.vari_best_class_name is NULL)
```

The light curves are downloaded using the *Gaia* Datalink service through the interface provided by the *astroquery* Python package [44]. *Gaia* DR3 offers epoch photometry data in the form of G , G_{BP} , and G_{RP} light curves, available as arrays in the DR3 `epoch_photometry` table. Only the G band is considered in this work. Observation times and magnitudes are extracted from the `g_transit_time` and `g_transit_mag` arrays, respectively. Although magnitude errors are not explicitly provided, they are derived using the `g_transit_flux_over_error` array. Finally, observations flagged as spurious are removed from the light curves by applying the `variability_flag_g_reject` array. This flag is the result of the operators described in Section 10.2.3 of the *Gaia* DR3 documentation [45].

Preprocessing and frequency extraction

A *Gaia* G band light curve is defined here as a sequence of observations $(t_j, m_j, e_j)_i$ with $j = 1, \dots, N_i$, where t is the time in days (d), m is the magnitude, e is the photometric error, and N_i is the number of observations of the i -th source. All sources are preprocessed as follows. Observations with $e_j > \bar{e} + 3\sigma_e$, where \bar{e} and σ_e are the mean and standard deviation of the photometric errors of the source, are removed. The magnitudes are subsequently centred by subtracting their mean, and the magnitudes and errors are rescaled by dividing them by the standard deviation of the magnitudes.

After preprocessing, the fundamental frequency of the source is estimated using the NUFFT implementation of the generalised LS periodogram [46–49]. The search is carried out on a linearly spaced frequency grid between $\nu_{\min} = 0.0007 \text{ d}^{-1}$ and $\nu_{\max} = 25 \text{ d}^{-1}$ with a step size of $\Delta_\nu = (10\Delta T)^{-1} \text{ d}^{-1}$, where $T = \max(t) - \min(t)$ is the total duration of the light curve. This configuration follows Section 10.2.3 of the *Gaia* documentation [45]. The frequencies associated with the ten highest local maxima of the periodogram are refined using a step size of $0.1\Delta_\nu$. Finally, the frequency associated with the highest periodogram peak ν_1 is saved for the next analysis. The FAP of the

periodogram peak associated with ν_1 is estimated using the Baluev approximation [41] through its implementation in the `astropy` Python library [50].

Variability models

The models associated with the periodic \mathcal{H}_P and red noise \mathcal{H}_R hypotheses are built using a GP framework. GPs are a generalisation of Gaussian probability distributions to functions that are widely used for nonparametric regression [51, 52]. The observed magnitudes in the light curves are modelled as

$$m_j = f(t_j) + \epsilon_j, \quad \forall j = 1, \dots, N_i \quad (1)$$

where $\epsilon_j \sim \mathcal{N}(0, e_j^2)$ and f is the function that we aim to model using GPs. More precisely, f is distributed as $\mathcal{N}(\mu, K_\phi)$, that is, a GP with a scalar mean μ and a covariance matrix with hyperparameters ϕ .

For \mathcal{H}_R , we use the exponential covariance function. Each element of the covariance matrix is defined as:

$$\kappa_R(t, t', \phi) = \sigma_R^2 \exp\left(-\frac{|t - t'|}{\tau}\right), \quad (2)$$

where $\phi = (\sigma_R^2, \tau)$ are the variance and the characteristic time scale, respectively. This covariance defines the DRW process and has been widely used to model stochastic variability in AGN studies [15, 17, 30, 31, 33, 34, 42]. The DRW power spectral density transitions from flat (white noise) to a power law f^{-2} (red noise) at the cutoff frequency $1/(2\pi\tau)$. Steeper frequency slopes have been reported for timescales of three months and less [36, 37], however, for the range of periods considered in this study, the DRW remains an appropriate baseline.

For \mathcal{H}_P , we adopt a sinusoidal covariance function:

$$\kappa_P(t, t', \phi) = \sigma_P^2 \cos(2\pi\nu(t - t')), \quad (3)$$

where $\phi = (\sigma_P^2, \nu)$ are the variance and the fundamental frequency of the variability, respectively.

For both hypotheses, the likelihood of the i -th source is given by

$$L_i(\theta) = -\frac{1}{2}(\bar{m}_i - \mu)^T \hat{K}_\phi^{-1}(\bar{m}_i - \mu) - \frac{1}{2} \log |\hat{K}_\phi| - \frac{N_i}{2} \log(2\pi), \quad (4)$$

where $\hat{K}_\phi = K_\phi + \text{diag}(\vec{e}_i^2) + I\sigma_N^2$ and $\theta = (\phi, \mu, \sigma_N)$ is the full parameter vector to be estimated. The full covariance considers two diagonal (white noise) terms, the first being fixed from the available photometric errors, while the second is inferred to account for possible underestimation of the former.

Parameter estimation

We infer the posterior of the model parameters

$$p(\theta|\mathcal{D}, \mathcal{H}) \propto L(\theta)p(\theta|\mathcal{H}), \quad (5)$$

using a MCMC approach based on the No-U-Turn Hamiltonian Monte Carlo algorithm [53]. The prior distribution $p(\theta|\mathcal{H})$ for each of the model parameters is defined as follows:

- Half-normal distribution with standard deviations of 1.5 and 0.5 for kernel standard deviations (σ_R, σ_P) and extra white noise (σ_N), respectively;
- Normal distribution with zero mean and unit variance for the mean μ ;
- Uniform distribution for the DRW time scale τ , bounded by the smallest and largest time differences in the light curve;
- Uniform distribution for the fundamental frequency ν , bounded by $\nu_1 \pm 1/(2T)$, where ν_1 is the LS periodogram estimate of the dominant frequency.

We run four independent MCMC chains of 1,000 samples each, discarding the first 500 samples (burn-in), yielding a total of 2,000 samples per parameter. The \hat{R} statistic [54], which compares the variances within and between chains, is used to assess the convergence of the MCMC algorithm. In this case, the light curves for which any given parameter yields $\hat{R} > 1.05$ are removed from the subsequent analysis.

The kernel functions of the GPs are implemented in JAX [55] and MCMC is performed using the NumPyro probabilistic programming library [56]. Just-in-time compilation is used when possible to accelerate computations. Under this setting, and for a *Gaia* light curve of average length, parameters are inferred in approximately 25 seconds on a CPU (single-core).

Evidence and Bayes factor

Robust comparison between the two competing hypotheses is carried out using the Bayes factor [57], which in our case is

$$\log B_{PR} = \log Z(D|\mathcal{H}_P) - \log Z(D|\mathcal{H}_R), \quad (6)$$

where

$$Z(D|\mathcal{H}) = \int L(\theta)p(\theta|\mathcal{H}) d\theta \quad (7)$$

is the Bayesian evidence. To efficiently compute the evidence, we use the learnt harmonic mean estimator [58]. This method overcomes the large variance of the traditional harmonic mean estimator by learning an optimal target distribution using a neural spline flow model [59, 60]. The model is trained using the full MCMC parameter trace and the values of the log posterior for each parameter combination. The default hyperparameters are used, except for the number of iterations, which is increased to 20. For a *Gaia* light curve of average length, the estimation of the evidence takes approximately 5 seconds on a CPU. Preliminary tests showed that the estimated evidence was within the error bars with respect to Nested Sampling-based methods [61], with only a fraction of the computational time required.

Selecting a threshold for the Bayes factor

Bayesian model selection is based on the posterior odds ratio, in this case

$$\frac{p(\mathcal{H}_P|D)}{p(\mathcal{H}_R|D)} = B_{PR} \frac{p(\mathcal{H}_P)}{p(\mathcal{H}_R)}. \quad (8)$$

Under the assumption of equally probable models (prior odds ratio equal to unity), the posterior odds ratio is equivalent to the Bayes factor and therefore $\log B_{PR} > 0$ can be taken as an indication that \mathcal{H}_P is more probable than \mathcal{H}_R . In practice, however, a more cautious threshold is used, such as the one based on the empirically calibrated Jeffrey scale [57].

In our work, we employ a simulation-based approach to establish an objective Bayes factor threshold. For this, we simulate pure DRW (red-noise) time series using the actual *Gaia* time stamps and photometric errors from the *Gaia* *G* light curves. We generate approximately 1 million synthetic time series and run the LS periodogram on each, recovering 89,248 simulations with estimated periods between 100 and $T/1.5$ days. After that, we apply the Bayesian inference procedures described above to effectively obtain a null distribution for the Bayes factor. From this distribution, we take the $100 \cdot (1 - \alpha)$ percentile as a threshold to select the final set of candidates. We adopt a conservative $\alpha = 0.001$ to ensure a highly pure selection of candidates.

Bayes factor as a function of the period of observation

In this section, we assess the plausibility of a pure DRW process mimicking a periodic signal based on their Bayes factor, B_{PR} , and examine how this changes with a longer observation period. To achieve this, we sampled 40,000 time series from the GP prior with a DRW kernel using a time vector with 80 observations spanning 2000 days to simulate the conditions of *Gaia* DR4. We then estimate their Bayes factors using both the complete time series and the first 1000 days (40 observations) of the data.

The distribution of the Bayes factor for these two scenarios is shown in the left panel of Figure A3 in orange and blue, respectively. Doubling the observation span causes a significant shift towards lower Bayes factors, reducing the fraction of positive log Bayes factors from 1.1% to 0.005%. The dashed black line indicates the simulation-based threshold used to select our final set of candidates. The middle panel of Figure A3 shows the only simulated time series that, when evaluated up to 1000 days, exceeds this threshold. Its log Bayes factor drops from 3.44 to -37.74 when evaluated over the full time span. No simulated time series exceeds the threshold when evaluated at full length. For reference, the right panel presents the simulated time series with the highest Bayes factor in

this scenario. Compared to *Gaia* DR3, future data releases will approximately double (DR4) and quadruple (DR5) the observational span, thereby reducing the chance of false positives due to red noise variability within the candidates period range, and allowing for less conservative thresholds to be used.

References

- [1] Begelman, M. C., Blandford, R. D. & Rees, M. J. Massive black hole binaries in active galactic nuclei. *Nature* **287**, 307–309 (1980).
- [2] Amaro-Seoane, P., Andrews, J., Arca Sedda, M. *et al.* Astrophysics with the Laser Interferometer Space Antenna. *Living Rev. Relativ.* **26**, 2 (2023).
- [3] Colpi, M., Danzmann, K., Hewitson, M. *et al.* LISA Definition Study Report. *arXiv e-prints* (2024).
- [4] Agazie, G., Anumarlapudi, A. & Archibald *et al.* (The Nanograv Collaboration), A. M. The NANOGrav 15 yr Data Set: Evidence for a Gravitational-wave Background. *Astrophys. J. Lett.* **951**, L8 (2023).
- [5] Xu, H. *et al.* Searching for the Nano-Hertz Stochastic Gravitational Wave Background with the Chinese Pulsar Timing Array Data Release I. *Res. Astron. Astrophys.* **23**, 075024 (2023).
- [6] Antoniadis, J., Arumugam, P. & Arumugam *et al.* (The EPTA and InPTA Collaborations), S. The second data release from the European Pulsar Timing Array. III. Search for gravitational wave signals. *Astron. Astrophys.* **678**, A50 (2023).
- [7] Reardon, D. J. *et al.* Search for an Isotropic Gravitational-wave Background with the Parkes Pulsar Timing Array. *Astrophys. J. Lett.* **951**, L6 (2023).
- [8] Shi, J.-M., Krolik, J. H., Lubow, S. H. & Hawley, J. F. Three-dimensional Magnetohydrodynamic Simulations of Circumbinary Accretion Disks: Disk Structures and Angular Momentum Transport. *Astrophys. J.* **749**, 118 (2012).
- [9] D’Orazio, D. J., Haiman, Z. & MacFadyen, A. Accretion into the central cavity of a circumbinary disc. *Mon. Not. R. Astron. Soc.* **436**, 2997–3020 (2013).
- [10] Westernacher-Schneider, J. R., Zrake, J., MacFadyen, A. & Haiman, Z. Multi-band light curves from eccentric accreting supermassive black hole binaries. *Phys. Rev. D* **106**, 103010 (2022).
- [11] D’Orazio, D. J., Haiman, Z. & Schiminovich, D. Relativistic boost as the cause of periodicity in a massive black-hole binary candidate. *Nature* **525**, 351–353 (2015).
- [12] Hu, B. X. *et al.* Spikey: self-lensing flares from eccentric SMBH binaries. *MNRAS* **495**, 4061–4070 (2020).
- [13] Davelaar, J. & Haiman, Z. Self-lensing flares from black hole binaries: General-relativistic ray tracing of black hole binaries. *Phys. Rev. D* **105**, 103010 (2022).
- [14] Graham, M. J. *et al.* A systematic search for close supermassive black hole binaries in the Catalina Real-time Transient Survey. *Mon. Not. R. Astron. Soc.* **453**, 1562–1576 (2015).
- [15] Charisi, M. *et al.* A population of short-period variable quasars from PTF as supermassive black hole binary candidates. *Mon. Not. R. Astron. Soc.* **463**, 2145–2171 (2016).
- [16] Liu, T., Gezari, S. & Miller, M. C. Did ASAS-SN Kill the Supermassive Black Hole Binary Candidate PG1302-102? *Astrophys. J. Lett.* **859**, L12 (2018).
- [17] Liu, T. *et al.* Supermassive Black Hole Binary Candidates from the Pan-STARRS1 Medium Deep Survey. *Astrophys. J.* **884**, 36 (2019).

- [18] Chen, Y.-J. *et al.* Searching for quasar candidates with periodic variations from the Zwicky Transient Facility: results and implications. *Mon. Not. R. Astron. Soc.* **527**, 12154–12177 (2024).
- [19] Sillanpaa, A., Haarala, S., Valtonen, M. J., Sundelius, B. & Byrd, G. G. OJ 287: Binary Pair of Supermassive Black Holes. *Astrophys. J.* **325**, 628 (1988).
- [20] D’Orazio, D. J., Haiman, Z. & Schiminovich, D. Relativistic boost as the cause of periodicity in a massive black-hole binary candidate. *Nature* **525**, 351–353 (2015).
- [21] Martí-Vidal, I. *et al.* Detection of jet precession in the active nucleus of M 81. *Astron. Astrophys.* **533**, A111 (2011).
- [22] von Fellenberg, S. D. *et al.* Radio jet precession in M 81*. *Astron. Astrophys.* **672**, L5 (2023).
- [23] Ivezić, Ž. *et al.* LSST: From Science Drivers to Reference Design and Anticipated Data Products. *Astrophys. J.* **873**, 111 (2019).
- [24] Haiman, Z. *et al.* Massive Black Hole Binaries as LISA Precursors in the Roman High Latitude Time Domain Survey. *arXiv e-prints* arXiv:2306.14990 (2023).
- [25] Gaia Collaboration *et al.* The Gaia mission. *Astron. Astrophys.* **595**, A1 (2016).
- [26] Hey, D. & Aerts, C. Confronting sparse Gaia DR3 photometry with TESS for a sample of around 60 000 OBAF-type pulsators. *Astron. Astrophys.* **688**, A93 (2024).
- [27] Gaia Collaboration *et al.* Gaia Data Release 3. Summary of the content and survey properties. *Astron. Astrophys.* **674**, A1 (2023).
- [28] Gaia Collaboration *et al.* Gaia Data Release 3. The extragalactic content. *Astron. Astrophys.* **674**, A41 (2023).
- [29] Gaia Collaboration *et al.* Gaia Early Data Release 3. The celestial reference frame (Gaia-CRF3). *Astron. Astrophys.* **667**, A148 (2022).
- [30] MacLeod, C. L. *et al.* Modeling the Time Variability of SDSS Stripe 82 Quasars as a Damped Random Walk. *Astrophys. J.* **721**, 1014–1033 (2010).
- [31] Vaughan, S. *et al.* False periodicities in quasar time-domain surveys. *Mon. Not. R. Astron. Soc.* **461**, 3145–3152 (2016).
- [32] Witt, C. A., Charisi, M., Taylor, S. R. & Burke-Spolaor, S. Quasars with Periodic Variability: Capabilities and Limitations of Bayesian Searches for Supermassive Black Hole Binaries in Time-domain Surveys. *Astrophys. J.* **936**, 89 (2022).
- [33] Kelly, B. C., Bechtold, J. & Siemiginowska, A. Are the Variations in Quasar Optical Flux Driven by Thermal Fluctuations? *Astrophys. J.* **698**, 895–910 (2009).
- [34] Kozłowski, S. *et al.* Quantifying Quasar Variability as Part of a General Approach to Classifying Continuously Varying Sources. *Astrophys. J.* **708**, 927–945 (2010).
- [35] Lin, A., Charisi, M. & Haiman, Z. Lomb-Scargle periodograms struggle with non-sinusoidal supermassive BH binary signatures in quasar lightcurves. *arXiv e-prints* arXiv:2505.14778 (2025).
- [36] Zu, Y., Kochanek, C. S., Kozłowski, S. & Udalski, A. Is Quasar Optical Variability a Damped Random Walk? *Astrophys. J.* **765**, 106 (2013).
- [37] Stone, Z. *et al.* Optical variability of quasars with 20-yr photometric light curves. *Mon. Not. R. Astron. Soc.* **514**, 164–184 (2022).

- [38] Holl, B. *et al.* Gaia Data Release 3. Gaia scan-angle-dependent signals and spurious periods. *Astron. Astrophys.* **674**, A25 (2023).
- [39] Rimoldini, L. *et al.* Gaia Data Release 3. All-sky classification of 12.4 million variable sources into 25 classes. *Astron. Astrophys.* **674**, A14 (2023).
- [40] Park, K., Xin, C., Davelaar, J. & Haiman, Z. Self-lensing flares from black hole binaries IV: the number of detectable shadows. *arXiv e-prints* arXiv:2409.04583 (2024).
- [41] Baluev, R. V. Assessing the statistical significance of periodogram peaks. *Mon. Not. R. Astron. Soc.* **385**, 1279–1285 (2008).
- [42] Zhu, X.-J. & Thrane, E. Toward the Unambiguous Identification of Supermassive Binary Black Holes through Bayesian Inference. *Astrophys. J.* **900**, 117 (2020).
- [43] Robnik, J. *et al.* Periodicity significance testing with null-signal templates: reassessment of PTF’s SMBH binary candidates. *Mon. Not. R. Astron. Soc.* **534**, 1609–1620 (2024).
- [44] Ginsburg, A. *et al.* astroquery: An Astronomical Web-querying Package in Python. *Astron. J.* **157**, 98 (2019).
- [45] Rimoldini, L. *et al.* Gaia DR3 documentation Chapter 10: Variability. Gaia DR3 documentation, European Space Agency; Gaia Data Processing and Analysis Consortium. Online at <https://gea.esac.esa.int/archive/documentation/GDR3/index.html>, id. 10 (2022).
- [46] Lomb, N. R. Least-Squares Frequency Analysis of Unequally Spaced Data. *Astrophys. Space Sci.* **39**, 447–462 (1976).
- [47] Scargle, J. D. Studies in astronomical time series analysis. II. Statistical aspects of spectral analysis of unevenly spaced data. *Astrophys. J.* **263**, 835–853 (1982).
- [48] Zechmeister, M. & Kürster, M. The generalised Lomb-Scargle periodogram. A new formalism for the floating-mean and Keplerian periodograms. *Astron. Astrophys.* **496**, 577–584 (2009).
- [49] Garrison, L. H., Foreman-Mackey, D., Shih, Y.-h. & Barnett, A. NIFTY-LS: Fast and Accurate Lomb–Scargle Periodograms Using a Non-uniform FFT. *Res. Notes Am. Astron. Soc.* **8**, 250 (2024).
- [50] Astropy Collaboration *et al.* The Astropy Project: Sustaining and Growing a Community-oriented Open-source Project and the Latest Major Release (v5.0) of the Core Package. *Astrophys. J.* **935**, 167 (2022).
- [51] Rasmussen, C. E. & Williams, C. K. I. *Gaussian Processes for Machine Learning* (The MIT Press, Cambridge, MA, 2006).
- [52] Aigrain, S. & Foreman-Mackey, D. Gaussian Process Regression for Astronomical Time Series. *Annu. Rev. Astron. Astrophys.* **61**, 329–371 (2023).
- [53] Hoffman, M. D. & Gelman, A. The No-U-Turn Sampler: Adaptively Setting Path Lengths in Hamiltonian Monte Carlo. *J. Mach. Learn. Res.* **15**, 1593–1623 (2014).
- [54] Gelman, A. & Rubin, D. B. Inference from Iterative Simulation Using Multiple Sequences. *Stat. Sci.* **7**, 457–472 (1992).
- [55] Bradbury, J. *et al.* JAX: composable transformations of Python+NumPy programs (2018). URL <http://github.com/jax-ml/jax>.
- [56] Phan, D., Pradhan, N. & Jankowiak, M. Composable Effects for Flexible and Accelerated Probabilistic Programming in NumPyro. *arXiv e-prints* arXiv:1912.11554 (2019).
- [57] Kass, R. E. & Raftery, A. E. Bayes factors. *J. Am. Stat. Assoc.* **90**, 773–795 (1995).

- [58] McEwen, J. D., Wallis, C. G. R., Price, M. A. & Spurio Mancini, A. Machine learning assisted Bayesian model comparison: learnt harmonic mean estimator. *arXiv e-prints* arXiv:2111.12720 (2021).
- [59] Durkan, C., Bekasov, A., Murray, I. & Papamakarios, G. Neural Spline Flows. *arXiv e-prints* arXiv:1906.04032 (2019).
- [60] Polanska, A., Price, M. A., Piras, D., Spurio Mancini, A. & McEwen, J. D. Learned harmonic mean estimation of the Bayesian evidence with normalizing flows. *arXiv e-prints* arXiv:2405.05969 (2024).
- [61] Albert, J. G. JAXNS: a high-performance nested sampling package based on JAX. *arXiv e-prints* arXiv:2012.15286 (2020).

Data availability. An electronic table listing the *Gaia* DR3 identifiers, the estimated Bayes factors, sky coordinates, and other relevant metadata is available online at cdsarc.cds.unistra.fr/GASP. The astronomical time series used in this study are publicly available and accessible via the *Gaia* archive: <https://gea.esac.esa.int/archive/>.

Code availability. The software and scripts to reproduce our results can be found in <https://github.com/IvS-KULeuven/GASP>. The libraries used to implement our pipeline are described in the previous section.

Acknowledgements. The Authors thank Phil Uttley and Zoltan Haiman for fruitful discussions. PH, JDR, and CA acknowledge the support from the BELgian federal Science Policy Office (BELSPO) through various PROgramme de Développement d’Expériences scientifiques (PRODEX) grants. CA acknowledges financial support from the Research Foundation Flanders under grant K802922N (Sabbatical leave). J.D. is supported by NASA through the NASA Hubble Fellowship grant HST-HF2-51552.001A, awarded by the Space Telescope Science Institute, which is operated by the Association of Universities for Research in Astronomy, Incorporated, under NASA contract NAS5-26555. CA and JD are grateful for the kind hospitality offered by the staff of the Center for Computational Astrophysics at the Flatiron Institute of the Simons Foundation in New York City, facilitating their initial encounters discussing this project in 2023. PH also acknowledges support from ANID – Millennium Science Initiative Program – ICN12_009 awarded to the Millennium Institute of Astrophysics MAS. This work has made use of data from the European Space Agency (ESA) mission *Gaia* (<https://www.cosmos.esa.int/gaia>), processed by the *Gaia* Data Processing and Analysis Consortium (DPAC, <https://www.cosmos.esa.int/web/gaia/dpac/consortium>). Funding for the DPAC has been provided by national institutions, in particular the institutions participating in the *Gaia* Multilateral Agreement. This work has made use of the Python package GaiaXPpy, developed and maintained by members of the *Gaia* Data Processing and Analysis Consortium (DPAC) and in particular, Coordination Unit 5 (CU5), and the Data Processing Centre located at the Institute of Astronomy, Cambridge, UK (DPCI).

Author contributions. CA, JDR, and JD came up with the idea of hunting for periodic variability in *Gaia* DR3 space photometry of AGN to discover SMBHBs and discussed all steps of the analyses and interpretations. PH designed, implemented, and applied all analysis methodologies, made all figures, and constructed GASP. JDR helped develop the methodological aspects while NJ provided context by performing SMBHB simulations. JD wrote the initial main text and PH wrote the initial Methods Section and the Appendix. All authors discussed the results, iterated upon the drafts, and contributed to the finetuning of the final version of the manuscript.

Competing interests. The authors declare no competing interests.

Appendix A Supporting figures and tables

Figure A1 displays the top 30 *Gaia* SMBHB candidates in terms of $\log_{10} B_{PR}$. Except for three, all of these candidates have periods within the range $[T/2.5, T/1.5]$ days. Figure A2 presents the top 30 candidates with the highest Bayes factor among the 39 cases with periods below $T/2.5$ (approximately 370 days).

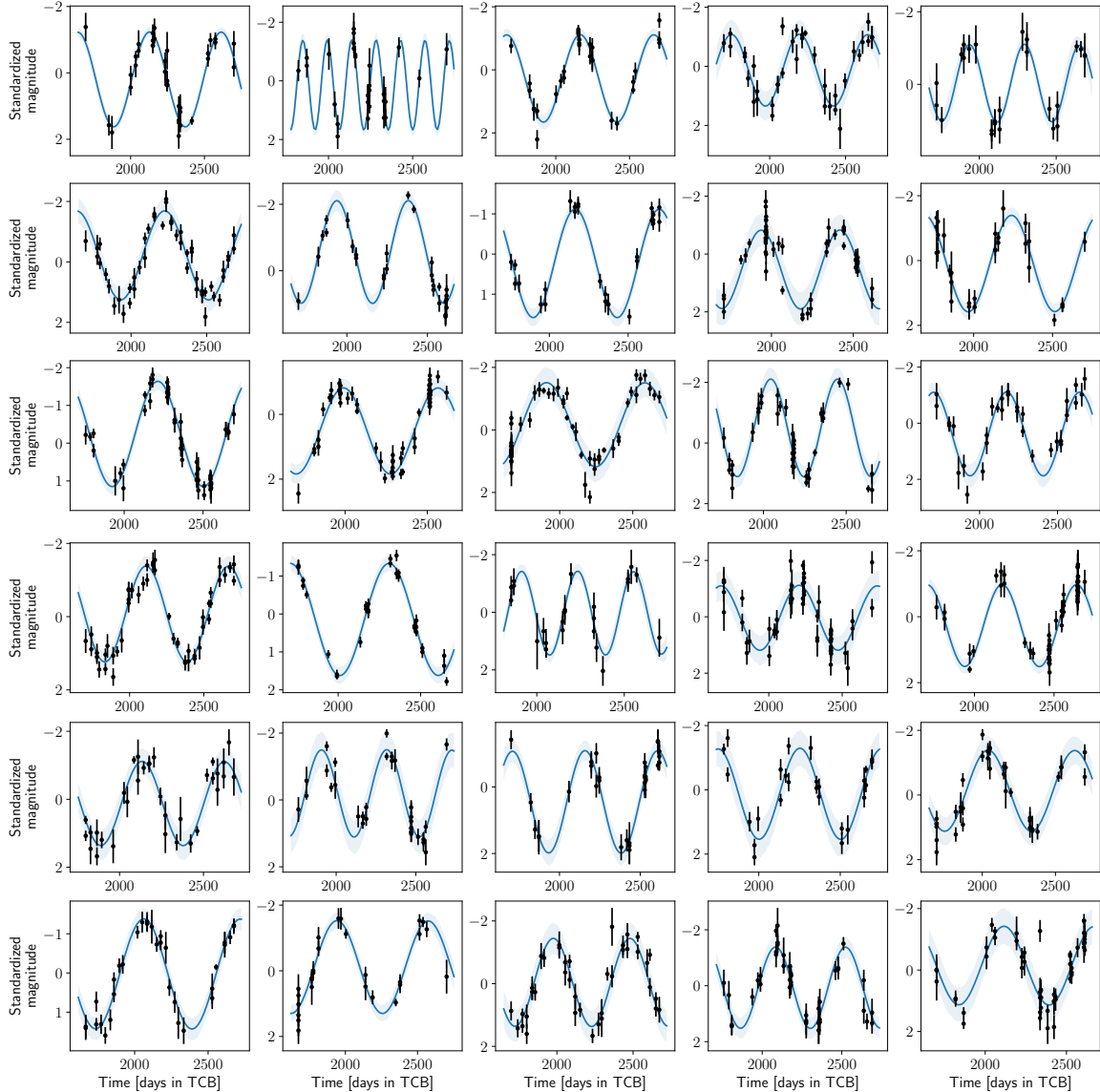


Fig. A1 The 30 *Gaia* sources with the highest $\log_{10} B_{PR}$ within the 48,472 subset of *Gaia* DR3 AGN. The GP posterior from the periodic model is shown in blue, where the solid line represents the median prediction while the shaded region denotes the 90% confidence interval. Measurements and their errors are shown in black. The objects are sorted by their Bayes factor, from highest to lowest.

Appendix B Generalization of the DRW model

In this work, we adopted the DRW model to represent stochastic, non-binary AGN variability. This model assumes a high-frequency slope of -2 in the power spectral density (PSD), however, some studies have found that this slope might be steeper for time scales of three months or less [36, 37]. To assess the impact of steeper PSD slopes on our results, we replace the exponential (DRW) covariance with a stretched-exponential covariance [36, 42]. Each element in this generalised covariance matrix is defined as:

$$\kappa_S(t, t', \phi) = \sigma_S^2 \exp\left(-\left|\frac{t-t'}{\tau}\right|^\gamma\right), \quad (\text{B1})$$

where $\gamma = 1$ recovers the DRW and $\gamma > 1$ produces slopes steeper than -2 in the PSD. In particular, $\gamma = 2$, which corresponds to a Gaussian covariance, exhibits an exponentially decreasing slope at high frequency [42]. We consider the cases $\gamma = 1.5$ and $\gamma = 2$ in this comparison, and compute the Bayes factors between the periodic hypothesis and these two new hypotheses for the 181 SMBHB candidates. Figure B4 shows the distribution of these Bayes factors, revealing a shift to lower values

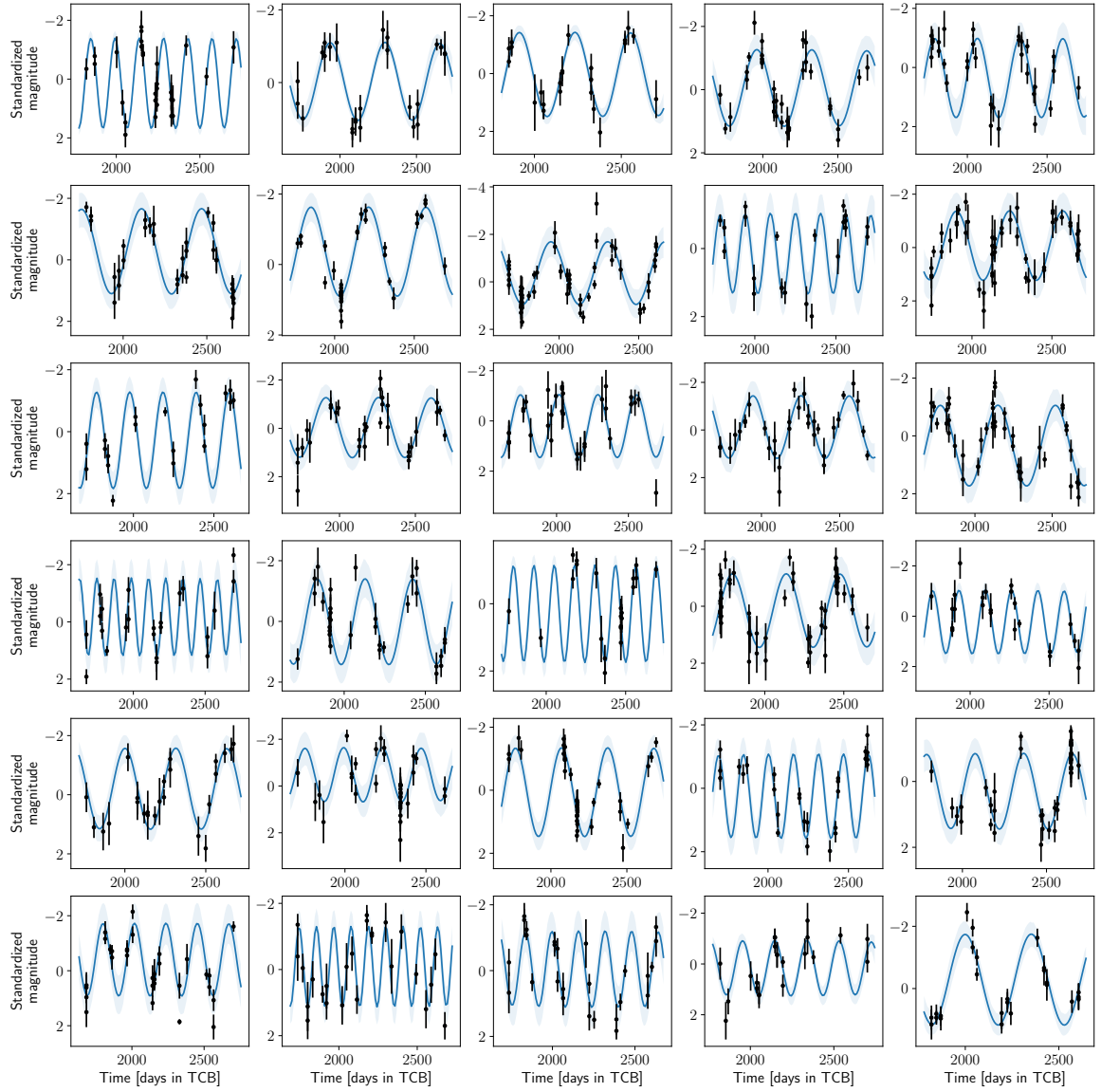


Fig. A2 Same as Fig. A1, but for the 30 *Gaia* AGN with periods below $T/2.5$ days (approximately 370 days).

with increasing γ . Nevertheless, for all the 181 candidates, the periodic hypothesis remains the one with the highest evidence, even in the extreme case of $\gamma = 2$.

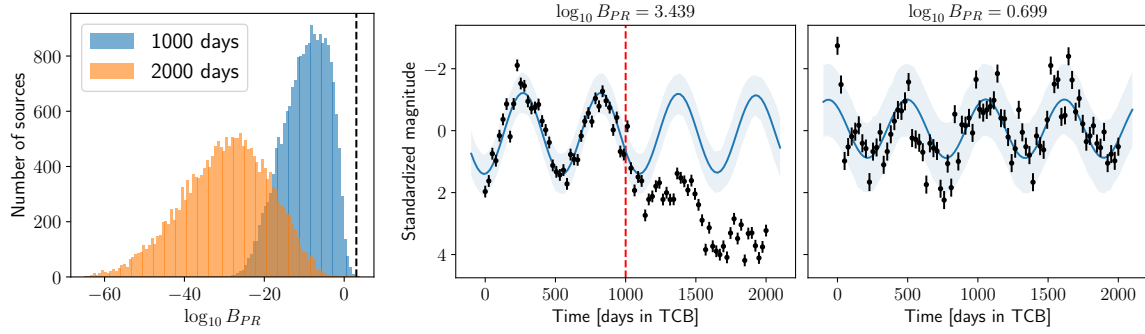


Fig. A3 Left panel: Histogram of the Bayes factor for the simulated DRW time series, computed over two time spans, up to 1000 days (blue) and over the full length of the data (orange). Extended observations reduce the chance of mistaking red noise for periodic signals. The dashed black line indicates the threshold value of 3.0423. Middle panel: The only simulated time series that exceeds this threshold when evaluated up to 1000 days (red dashed line). Its estimated period is 548 ± 29 days. Right panel: No full-length simulated time series exceeds the threshold; however, the simulation with the highest Bayes factor is displayed for comparison. Its estimated period is 561 ± 7 days.

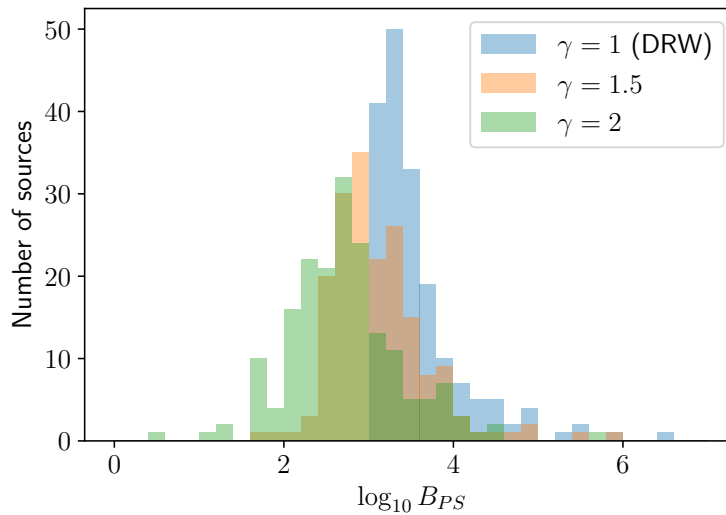


Fig. B4 Distribution of the logarithmic Bayes factor for the 181 SMBHB candidates comparing the periodic covariance against the stretched-exponential covariance. The evidence for the periodic hypothesis is always the highest, regardless of the exponent γ .